

Unlocking plasmonic nanolaser performance via exciton-plasmon interaction dynamics

Ru Wang(王茹), Daotong You(游道通), Zhuxin Li(李竹新), Chuansheng Xia(夏传晟), Xiaoxuan Wang(王潇璇), Feifei Qin(秦飞飞), and Chunxiang Xu(徐春祥)

Citation: Chin. Phys. B, 2026, 35 (**2**): 024206. DOI: 10.1088/1674-1056/ae27b5
http://cpb.iphy.ac.cn; http://iopscience.iop.org/cpb

What follows is a list of articles you may be interested in

Highly sensitive, multi-stage, and mid-infrared refractive index sensor based on photonic spin Hall effect

Jiaye Ding(丁嘉烨), Chenglong Wang(汪承龙), Shengli Liu(刘胜利), Peng Dong(董鹏), and Jie Cheng(程杰)
Chin. Phys. B, 2026, 35 (**1**): 014201. DOI: 10.1088/1674-1056/ade24c

Giant enhancement of negative friction by resonant coupling between localized surface phonon polaritons and graphene plasmonics

Kaipeng Liu(柳开鹏), Shuai Zhou(周帅), Shiwei Dai(戴士为), and Lixin Ge(葛力新)
Chin. Phys. B, 2025, 34 (**1**): 014202. DOI: 10.1088/1674-1056/ad886c

Light-field modulation and optimization near metal nanostructures utilizing spatial light modulators

Zini Cao(曹子倪), Hai Lin(林海), Yuqing Cheng(程宇清), Yixuan Xu(徐艺轩), Qihuang Gong(龚旗煌), and Guowei Lü(吕国伟)
Chin. Phys. B, 2024, 33 (**10**): 104201. DOI: 10.1088/1674-1056/ad6555

Surface phonon resonance: A new mechanism for enhancing photonic spin Hall effect and refractive index sensor

Jie Cheng(程杰), Chenglong Wang(汪承龙), Yiming Li(李一铭), Yalin Zhang(张亚林), Shengli Liu(刘胜利), and Peng Dong(董鹏)
Chin. Phys. B, 2024, 33 (**8**): 084201. DOI: 10.1088/1674-1056/ad4a3c

Tunable artificial plasmonic nanolaser with wide spectrum emission operating at room temperature

Peng Zhou(周鹏), Jia-Qi Guo(郭佳琦), Kun Liang(梁琨), Lei Jin(金磊), Xiong-Yu Liang(梁熊玉), Jun-Qiang Li(李俊强), Xu-Yan Deng(邓绪彦), Jian-Yu Qin(秦建宇), Jia-Sen Zhang(张家森), and Li Yu(于丽)
Chin. Phys. B, 2024, 33 (**5**): 054210. DOI: 10.1088/1674-1056/ad2dca

---

Unlocking plasmonic nanolaser performance via exciton–plasmon interaction dynamics

Ru Wang(王茹)[1,†], Daotong You(游道通)[3], Zhuxin Li(李竹新)[4], Chuansheng Xia(夏传晟)[5], Xiaoxuan Wang(王潇璇)[5], Feifei Qin(秦飞飞)[6], and Chunxiang Xu(徐春祥)[2,‡]

[1] *College of Physics and Electronic Engineering, Shanxi Normal University, Taiyuan* 030031, *China*
[2] *School of Electronic Science and Engineering, Southeast University, Nanjing* 211189, *China*
[3] *Guangxi Key Laboratory of Optoelectronic Information Processing, School of Optoelectronic Engineering, Guilin University of Electronic Technology, Guilin* 541004, *China*
[4] *School of Mathematics and Physics, Anhui Jianzhu University, Hefei* 230031, *China*
[5] *School of Biological Science and Medical Engineering, Southeast University, Nanjing* 210096, *China*
[6] *GaN Optoelectronic Integration International Cooperation Joint Laboratory of Jiangsu Province, Nanjing University of Posts and Telecommunications, Nanjing* 210003, *China*

(Received 14 October 2025; revised manuscript received 3 December 2025; accepted manuscript online 4 December 2025)

Plasmonic nanolasers are transitioning from empirical optimization to a new paradigm driven by physical mechanisms. Owing to the lack of guidance from internal mechanisms, this transformation process remains highly challenging. Therefore, elucidating the governing nanoscale light–matter interactions has become essential for unlocking their full performance potential. In this paper, we establish a framework that connects the strength of exciton–plasmon interactions with plasmonic nanolaser performance. The evolution of the laser spectrum under increasing pumping fluence, reflected by variations in intensity, spectral peak position, and full width at half maximum, provides clear evidence of exciton–plasmon interactions. These interactions are further verified by changes in the emission lifetime with incident fluence, and it is found that the lifetime variation correlates with the change in spectral full width at half maximum. Furthermore, we calculate and analyze various loss mechanisms in plasmonic nanolasers, revealing how the strength of exciton–plasmon interactions actively modulates optical loss channels and fundamentally controls the lasing threshold. Understanding exciton–plasmon interaction dynamics is not merely a theoretical pursuit but a critical step toward realizing truly practical and scalable nanophotonic devices.

Keywords: surface plasmon, nanolaser, linewidth, threshold, loss

PACS: 42.55.Px, 78.47.D–, 73.40.Qv

DOI: 10.1088/1674-1056/ae27b5 **CSTR:** 32038.14.CPB.ae27b5

1. Introduction

In order to achieve integration with next-generation technologies such as on-chip optical interconnection,[1] quantum communication networks,[2] and ultra-sensitive biosensors,[3–5] laser devices need to be miniaturized, but they now face a fundamental barrier: the diffraction limit of light. With the decrease in the physical size of conventional lasers, the mode volume gradually becomes smaller, and the performance suffers a catastrophic decline due to the diffraction limit. Plasmonic nanolasers emerge as a transformative solution by harnessing surface plasmons (SPs) to confine light far below the diffraction limit.[6] These devices exploit hybrid light–matter interactions within subwavelength cavities, typically comprising semiconductor gain media coupled to metallic nanostructures, thereby realizing lasing behavior. As device dimensions approach molecular scales, quantum effects dominate, rendering traditional gain models obsolete and necessitating a fundamental re-examination of energy transfer pathways at the nanoscale. Ning[7] discussed that there is no difference in the essential physics between the "SPP-laser" regime and the spaser regime and compared the key similarities and differences between gain models of conventional lasers and plasmonic lasers. Their performance is critically governed by two interdependent metrics: the lasing threshold and spectral linewidth. The former dictates power efficiency and thermal management, while the latter determines signal fidelity for applications requiring precise spectral control. Crucially, both parameters originate from the gain mechanism — a complex interplay between excitons in semiconductors and plasmons in metals.[8,9] Understanding exciton–plasmon interaction dynamics is not merely a theoretical pursuit but a critical step toward unlocking truly practical and scalable nanophotonic devices. The pursuit of ultracompact coherent light sources has long been constrained by the empirical nature of nanolaser development. Therefore, it is necessary to establish a basic paradigm shift: exciton–plasmon interaction

[†]Corresponding author. E-mail: wangru@sxnu.edu.cn
[‡]Corresponding author. E-mail: xcxseu@seu.edu.cn

© 2026 Chinese Physical Society and IOP Publishing Ltd. All rights, including for text and data mining, AI training, and similar technologies, are reserved.

dynamics serve as the universal governing principle underlying all key performance metrics in plasmonic nanolasers.

In recent years, researchers have successively realized ultraviolet to infrared plasmonic nanolasers using iterative optimization of materials and composite structures.[6,10–15] Among these efforts, progress has been made in inferring the gain mechanism of optimized plasmonic nanolasers from changes in laser performance.[16–18] For example, Lu *et al.*[19] observed a lasing mode shift relative to a photonic nanolaser mode by using a plasmonic nanolaser with an optimized structure. By calculating the carrier density and carrier lifetime, it was proposed that the gain mechanism of the plasmonic nanolaser originates from the coupling between surface plasmons and excitons, rather than from the electron–hole plasma mechanism. Yet, how exciton–plasmon interaction dynamics affect the spectral linewidth through changes in the exciton recombination rate lacks theoretical guidance. Apart from the gain mechanism, the loss mechanism is also a crucial factor determining nanolaser performance, which is mainly reflected in the lasing threshold. It is well known that processes such as metal absorption, radiation leakage, and nonradiative recombination can significantly degrade nanolaser performance. Wang *et al.*[20] quantitatively revealed that the loss sources of plasmonic nanolasers include material loss, metal loss, and radiation loss. This provides important guidance for optimizing both the cavity and gain materials of plasmonic nanolasers. Although loss-reduction strategies show clear benefits, models linking interaction-strength modulation of optical loss to the lasing threshold remain incomplete. Current optimization methods therefore remain dependent on trial-and-error-based material substitutions and structural modifications due to the absence of physics-based models capable of predicting nanoscale interactions. This inherent limitation hinders device reproducibility and application-specific optimization. Therefore, there is an urgent need to establish a comprehensive link between the fundamental exciton–plasmon interaction, the resulting laser performance (including threshold and linewidth), and the practical viability of these devices.

In this paper, a framework correlating the measured interaction strength with the performance of semiconductor/insulator/metal plasmonic nanolasers (ZnO/Al_2O_3/Ag) is established. Through systematic characterization of key performance parameters such as threshold, full width at half maximum (FWHM), and emission intensity, combined with correlation analysis between the recombination lifetime and the interaction strength extracted from laser dynamics measurements, it is further verified that performance variations of the nanolaser originate from modulation of the exciton–plasmon interaction strength. Theoretical calculations further elucidate the mechanism by which interaction strength governs spectral linewidth broadening. Moreover, various optical loss channels are analyzed using a two-energy-level system, demonstrating how exciton–plasmon interaction strength dynamically modulates these losses and thereby controls the threshold intensity. This fundamental insight into interaction-dependent gain and loss mechanisms provides a theoretical framework for optimizing plasmonic nanolaser performance and broadening their application scope.

2. Theoretical method and experiment

2.1. Sample preparation

The single-crystalline ZnO nanowire array was produced using chemical vapor deposition (CVD), similar to our previously reported method.[21] A 100 nm thick Ag thin film was deposited on a silicon substrate by electron-beam evaporation, and an approximately 5 nm thick Al_2O_3 layer was deposited on the Ag film by atomic layer deposition (ALD). The ZnO nanowire array was dispersed in an absolute alcohol solution using ultrasonic oscillation, and the resulting solution was drop-cast onto the Al_2O_3/Ag substrate.

2.2. Optical measurement and simulation

The ZnO nanorod morphologies were characterized using a scanning electron microscope (SEM) (Carl Zeiss Ultra Plus). The refractive index of the ZnO film was measured by spectroscopic ellipsometry (SE-m). The ZnO plasmonic nanocavity was optically pumped using a 325 nm femtosecond (fs) laser (pulse duration of 100 fs and repetition rate of 1000 Hz), which was focused by a microscope objective (40×), resulting in a pumping beam diameter of approximately 4 μm. The photoluminescence (PL), lasing performance, and PL decay lifetime of the samples were detected using an optical multichannel analyzer (OMA) system (Princeton, Acton SP2500i) and an optically triggered streak camera system (Optronic GmbH SC-10). Theoretical calculations and simulations were carried out using the finite-difference time-domain (FDTD) method, in which the Helmholtz equation was solved with absorbing boundary conditions.

3. Results and discussion

3.1. Lasing behavior of ZnO plasmonic nanolaser

As shown in Fig. 1(a), the dispersion curves of the composite nanocavity formed by an approximately 7 μm long ZnO nanowire (diameter of approximately 150 nm) placed on an Al_2O_3/Ag substrate were calculated. The effective index of the fundamental hybrid mode in the composite nanocavity is much larger than that of the SP mode formed at the Al_2O_3/Ag interface within the ZnO luminescence spectrum. As shown in the inset of Fig. 1(a), the higher effective index of the ZnO/Al_2O_3/Ag nanocavity indicates stronger optical field confinement, leading to higher confined energy, a

smaller mode area, and a larger confinement factor. As shown in Fig. 1(b), an incident wave at the left plane generates a surface plasmon mode with a standing-wave pattern inside the nanowire cavity. Since the radiation field of the displaced continuous cavity mode consists of photons scattered into free space and surface plasmons propagating along the metal surface outside the cavity, both radiation components are collected by the objective lens in the experiment. The lower right corner of Fig. 1(b) shows an SEM image of a ZnO nanowire placed on an Ag/Al_2O_3 substrate.

Subsequently, the constructed devices were characterized spectrally. Figure 1(c) shows the spectra of a ZnO plasmonic nanolaser collected from a micro-region. When the pumping fluence is lower than 24.5 μJ/cm^2, the spectrum exhibits broad spontaneous emission. Above 24.5 μJ/cm^2, the spectrum rapidly narrows and transitions into laser emission. Thus, the lasing threshold is determined to be 24.5 μJ/cm^2. With increasing fluence density, the central peak of the spectrum exhibits a blueshift. Meanwhile, an exciton peak is observed at 3.323 eV (Fig. 1(d)).

In addition, when the lasing mode appears, the operation of the plasmonic nanolaser can be further verified by measuring the polarization of the laser mode. As shown in Fig. 1(e), the polarization direction is consistent with the orientation of the nanowire. These longitudinal lasing modes, namely the fundamental hybrid mode, confirm that the device operates as a plasmonic nanolaser. During operation, the relationship between the variation of the lasing peak and the FWHM requires further investigation.

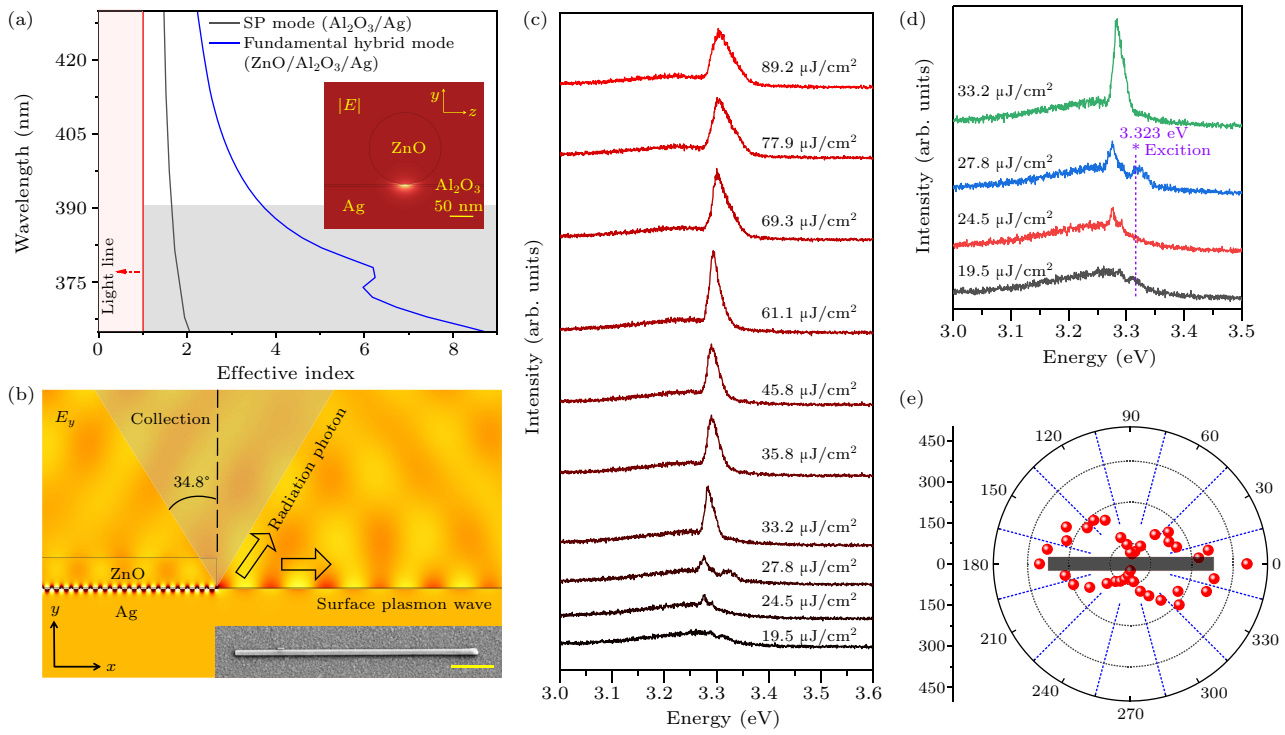


Fig. 1. (a) Dispersion curves of the fundamental hybrid mode in the ZnO/Al_2O_3/Ag nanocavity and the SP mode formed at the Al_2O_3/Ag interface (inset: cross-sectional field distribution); (b) Output coupling of a ZnO plasmonic nanolaser (SEM image of the device is shown in the lower right corner; scale bar: 1 μm); (c) Spectra under different pumping fluences; (d) Low-fluence amplification spectrum, where the exciton peak is located at 3.323 eV; (e) Relationship between the far-field emission intensity and polarization angle of the plasmonic nanolaser.

3.2. Laser performance parameter of plasmonic nanolaser

The relationship between the incident fluence and the spectral characteristics — including peak intensity, peak position, and FWHM — is illustrated in Figs. 2(a)–2(c). Two distinct demarcation points are observed in Figs. 2(a)–2(c): one corresponds to the lasing threshold, and the other is located at 61.6 μJ/cm^2. As the pumping fluence increases, the peak intensity of the spectrum also increases, reaching its maximum at a pumping fluence of 61.1 μJ/cm^2. When the pumping fluence reaches 61.1 μJ/cm^2, the peak position stabilizes. Regarding the FWHM, it narrows after surpassing the lasing threshold, indicating that the lasing mode within the cavity has reached a steady state. When the pumping fluence exceeds 61.6 μJ/cm^2, the laser intensity decreases, the FWHM of the lasing mode begins to broaden, and a sudden enhancement of the blueshift is observed in Fig. 2(b). These changes suggest that the lasing mode inside the cavity becomes unstable, leading to degraded laser performance.

As shown in Fig. 2(d), for the optically pumped laser, when light is incident on the device, electrons in the semiconductor material are excited to higher-energy electron–hole pair states and subsequently relax to the working level, as in-

dicated by the green arrows, forming excitons. Photon emission is strongly quenched due to resonant energy transfer to SP modes, as indicated by the red arrows in the panel. The excitons recombine and emit surface plasmons at the Al_2O_3/Ag interface. The plasmonic oscillations at the Al_2O_3/Ag interface stimulate this emission, providing feedback for the spasing action (as indicated by the hollow arrows). When the pumping fluence reaches the threshold, the emission of the laser mode becomes stable, and the entire system enters a strong SP–exciton interaction regime. However, when the pumping fluence exceeds 61.1 μJ/cm^2, the spectral intensity decreases significantly, the peak exhibits a rapid blueshift, and the FWHM broadens. Here, we hypothesize a weakening of the SP–exciton interaction.

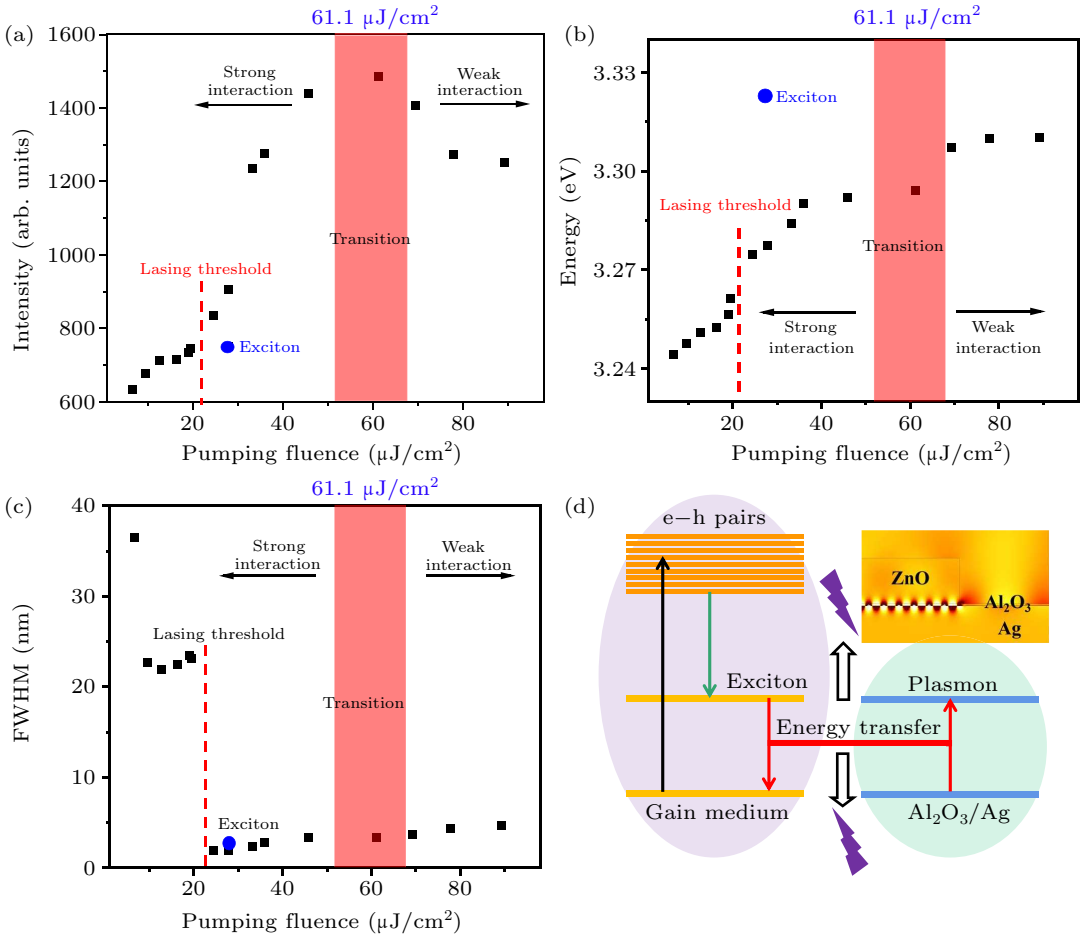


Fig. 2. (a) Relationship between pumping fluence and light intensity of a ZnO plasmonic nanolaser. (b) Relationship between pumping fluence and lasing peak position of a ZnO plasmonic nanolaser. (c) Relationship between pumping fluence and FWHM of a ZnO plasmonic nanolaser. (d) Schematic illustration of the operating principle of the plasmonic nanolaser (inset: output coupling of a ZnO plasmonic nanolaser).

3.3. Exciton–plasmon interaction dynamics

To further verify this hypothesis, time-resolved photoluminescence spectra were measured at different pumping fluences to characterize the interaction strength, as shown in Fig. 3(a). With increasing pumping fluence, the spectrum exhibits a blueshift, consistent with the spectral blueshift observed in Fig. 2(b). As shown by the fluorescence lifetime fitting curve at 19.5 μJ/cm^2 (below the threshold) in Fig. 3(b), the decay process is relatively slow. In contrast, for the fluorescence lifetime fitting curve at 27.8 μJ/cm^2 (above the threshold), the exciton recombination lifetime of 86 ps exhibits a significantly faster decay. This behavior arises because, after reaching the threshold, the probability of radiative transitions increases. In addition, resonance between plasmons and excitons enhances the exciton transition rate, enabling propagation within a cavity with dimensions smaller than half the wavelength. According to the statistics of the fitted lifetimes under all pumping fluences shown in Fig. 3(c), the lifetime gradually decreases with increasing fluence, which is consistent with the operating mechanism of plasmonic nanolasers. However, at pumping fluences exceeding 61.6 μJ/cm^2, the fitted lifetimes suddenly increase. This phenomenon may be attributed to a weakening of the energy resonance between plasmons and excitons, which slows down the transition rate.

This phenomenon can be explained by the following expression:[9]

$$\Delta\omega_{las} = \frac{1}{\tau_p} - \frac{\beta}{n_s \tau_{rad}} n_2, \tag{1}$$

where $\Delta\omega_{las}$ is the laser linewidth, τ_p is the photon lifetime in the cavity, β is the spontaneous emission factor, n_s =

$n_2/(n_2-n_1)$ is the incomplete population inversion factor, τ_{rad} is the radiative lifetime, and n_1 and n_2 are the numbers of particles in the lower and higher energy levels, respectively. With increasing pumping fluence, the laser linewidth is governed by the photon lifetime, radiative lifetime, spontaneous emission factor, and particle population when the lasing state is reached. In the lasing regime, the photon lifetime and particle population tend to reach a dynamic balance. According to Eq. (1), when the laser linewidth $\Delta\omega_{las}$ broadens, the radiative lifetime τ_{rad} increases, indicating a weakening of the energy resonance between plasmons and excitons. This further demonstrates that the laser characteristics are strongly influenced by exciton–plasmon interactions.

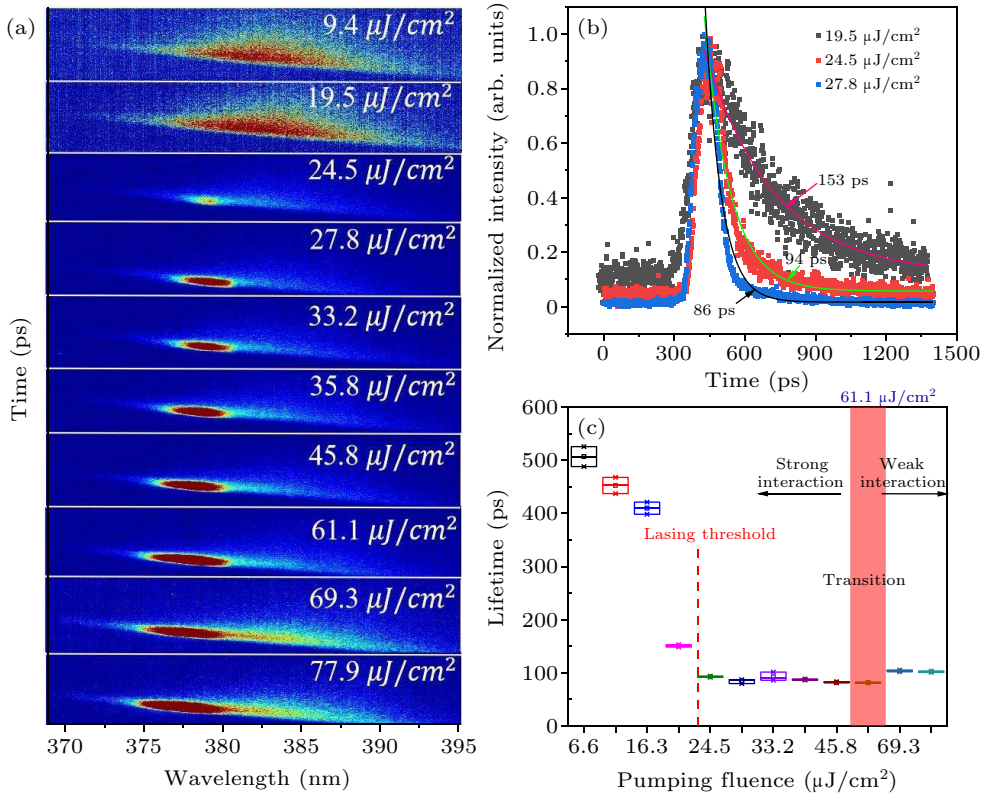


Fig. 3. (a) Time-resolved fluorescence spectra under different pumping fluences (ordinate range: 0–1400 ps). (b) Time-dependent intensities at pumping fluences of 19.5 μJ/cm^2 (black), 24.5 μJ/cm^2 (red), and 27.8 μJ/cm^2 (blue). (c) The relationship between PL attenuation lifetime and pumping fluence.

3.4. Loss influenced lasing threshold

Furthermore, we discuss the loss factors that affect the lasing threshold. The various losses of a plasmonic nanolaser are further explained below. Theoretically, the modal loss can be calculated using the following formula:[22]

$$\alpha_i = \frac{\omega\varepsilon_0}{2P_z}\int_A \mathrm{d}\hat{\rho}\,\mathrm{Im}\left[\varepsilon(\hat{\rho},\hbar\omega)\right]|E(\hat{\rho})|^2$$
$$= \frac{1}{2\eta_0 P_z}\int_A \mathrm{d}\hat{\rho}\,|E(\hat{\rho})|^2 n_r(\hat{\rho},\omega)\,\alpha(\hat{\rho},\hbar\omega), \quad (2)$$

$$P_z = \int_A \mathrm{d}\hat{\rho}\,\frac{1}{2}\mathrm{Re}\left[E(\hat{\rho})\times H(\hat{\rho})\right]\cdot\hat{z}, \quad (3)$$

where A is the cross section of the waveguide device; $\hat{\rho}$ is the position vector; P_z is the time-averaged power flow of the mode; $\varepsilon(\hat{\rho},\hbar\omega)$, $n_r(\hat{\rho},\hbar\omega)$, and $\alpha(\hat{\rho},\hbar\omega)$ are the space-dependent real part of the material permittivity, material refractive index, and material absorption, respectively; $\eta_0(=\sqrt{\mu_0}/\varepsilon_0)$ is the intrinsic impedance. The imaginary part of the dielectric constant of the metal strongly influences the modal loss in Eqs. (2) and (3), representing the extinction coefficient and determining light absorption in the metal. Therefore, the metal loss (including electron scattering and inter/intraband transitions) can be expressed by the modal loss.

The mirror loss can be calculated by

$$\ln(1/R)/L, \quad (4)$$

where the two facets are assumed to have the same reflectivity R, which depends on the refractive index. This is also referred to as radiation loss, which more clearly describes the formation process of the laser. Equations (2)–(4) theoretically describe the relationship between refractive index and loss coefficient. In the refractive index range 2.4–2.495, as shown in Fig. 4(a), metal losses range from 10507 cm^{-1} to 8970 cm^{-1}, while radiation losses range from 2957 cm^{-1} to 2830 cm^{-1}. It is clear that metal losses account for a larger proportion than radiation losses, indicating that the plasmonic cavity is primarily affected by metal loss. Strong exciton–plasmon interaction can overcome radiation and metal losses, thereby enabling the

emergence of laser behavior.

For the lasing mode, in Fig. 4(b), the relationship between the quality factor Q and the total loss is calculated by $\frac{\omega}{\Gamma}Qv_g$,[20] where ω is the resonance frequency, Γ is the confinement factor, and v_g is the cavity mode group velocity. With $\omega = 4.99 \times 10^{15}$ rad/s, $\Gamma = 0.429$, and $v_g = 1.22 \times 10^8$ m/s, the total loss for Q values from 10 to 100 is 94928 cm^{-1} to 9492 cm^{-1}. Clearly, a high quality factor corresponds to low loss. To reduce the lasing threshold, a high quality factor is crucial and can be achieved through cavity design. In addition to metal and radiation losses, there is still excess loss. Intraband free-carrier absorption, also known as the plasma effect, is modeled as being directly proportional to the carrier concentration and the square of the wavelength. As pumping fluence increases, free-carrier plasma effects reduce the refractive index of the materials, resulting in a blueshift.[23]

As shown in Fig. 4(c), absorption loss in plasmonic nanolasers can be understood via the energy level diagram of self-absorption of the working material. This loss also contributes to weakening the exciton–plasmon interaction. In Fig. 4(d), when incident light irradiates the plasmonic nanocavity, carriers are first absorbed by the material itself and surface plasmons. As pumping fluence increases, the mode just overcomes metal losses, and the exciton–plasmon interaction gradually intensifies. Therefore, reducing metal losses to obtain low-threshold plasmonic nanolasers can be achieved by optimizing the metal surface structure and decreasing internal metal losses (e.g., reducing temperature). When pumping fluence increases further, radiation loss becomes significant and laser behavior is observed. However, when pumping fluence exceeds 61.1 μJ/cm^2, self-absorption in the gain material leads to weakening of the exciton–plasmon interaction. By using high-quality semiconductor materials and optimized structures, radiation loss and material self-absorption can be reduced, allowing targeted optimizations for future device applications.

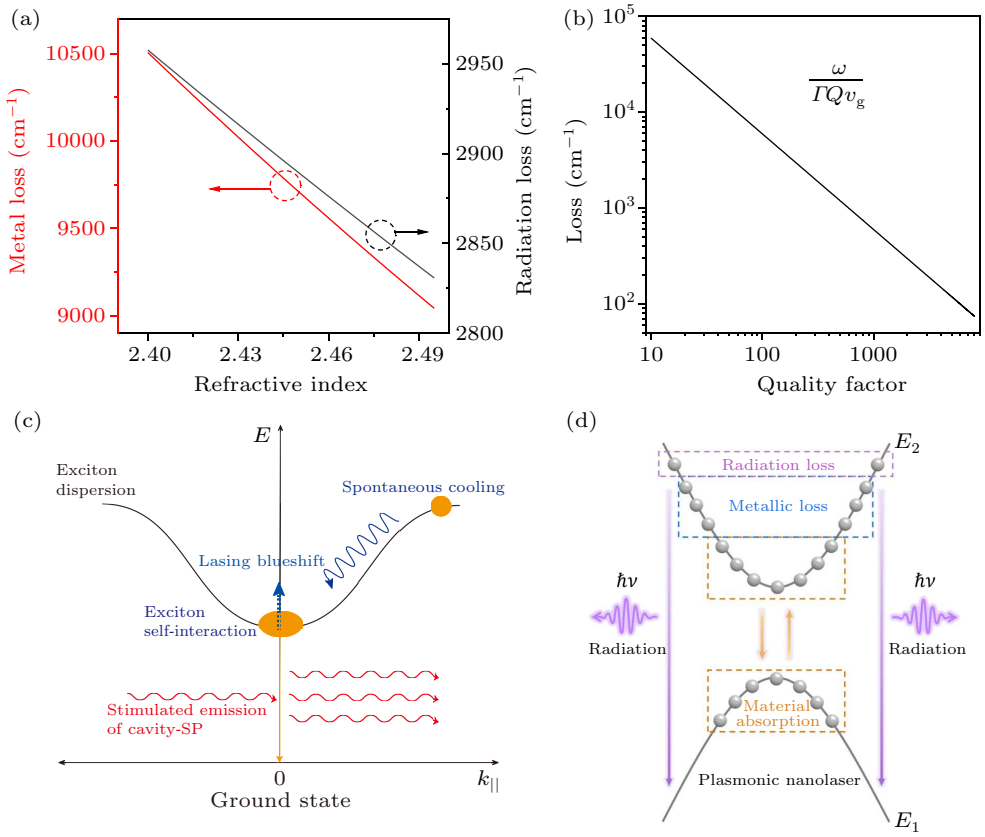


Fig. 4. (a) Calculated relationship between refractive index, metal loss, and radiation loss in a plasmonic nanolaser. (b) Relationship between quality factor Q and total loss of plasmonic nanolasers. (c) Energy level diagram illustrating self-absorption of the working material in the plasmonic nanolaser. (d) Schematic diagram of the gain–loss competition mechanism in a plasmonic nanolaser.

4. Conclusion

In conclusion, the performance of plasmonic nanolasers is unlocked through deciphering exciton–plasmon interaction dynamics. It is demonstrated that interaction strength serves as the master key controlling both spectral characteristics (via linewidth broadening) and power efficiency (through threshold modulation). By observing the lasing performance of ZnO plasmonic nanolasers, it was found that the lasing behavior first enhances and then attenuates with increasing incident pumping fluence. This behavior is closely related to changes in exciton–plasmon interaction strength.

Furthermore, through systematic analysis of the correla-

tion between recombination lifetime and interaction strength during the lasing evolution process, the critical role of this coupling mechanism in modulating laser performance was confirmed. Theoretical calculations further establish the mechanism by which interaction strength governs spectral linewidth broadening. It is found that weakening of the energy resonance between plasmons and excitons leads to linewidth broadening in plasmonic nanolasers.

Moreover, the sources of various losses in plasmonic nanolasers were analyzed. Through a two-level system model, interaction strength is shown to dynamically reconfigure optical losses — including metal loss, radiation loss, and material self-absorption — to determine the lasing threshold. This theoretical framework transforms device optimization from empirical tuning to predictive design: by strategically engineering interaction strength through material selection and nanostructure design, devices can be tailored for specific application requirements.

Acknowledgments

This project was supported by the Natural Science Foundation of Anhui Jianzhu University (Grant No. 2023QDZ05), the National Natural Science Foundation of China (Grant Nos. 62204127 and 12304453), and the Shanxi Province Science Foundation for Youths (Grant No. 202503021212220).

References

[1] Liang Y, Li C, Huang Y Z and Zhang Q 2020 *ACS Nano* **14** 14375
[2] Ma R M and Wang S Y 2021 *Nanophotonics* **10** 3623
[3] Ma R M and Oulton R F 2019 *Nat. Nanotechnol.* **14** 12
[4] Zhao D, Wang X, Chen Y, Rao X, Gao J, Qi Y, Yang H and Zheng X 2025 *Opt. Commun.* **596** 132421
[5] Gao J, Wang X, Chen Y, Zhao D, Qi Y and Yang H 2025 *J. Opt. Soc. Am. B* **42** 742
[6] Ellis T C, Eslami S and Palomba S 2024 *Nanophotonics* **13** 2707
[7] Ning C Z 2021 *Nanophotonics* **10** 3619
[8] Wang R, Wang C, Ma Y, Sun J, Yan P, Xu C and Pan C 2023 *Adv. Opt. Mater.* **11** 2203137
[9] Khurgin J B and Noginov M A 2021 *Laser Photonics Rev.* **15** 2000250
[10] Li H, Huang Z T, Hong K B, Hsu C Y, Chen J W, Cheng C W, Chen K P, Lin T R, Gwo S J and Lu T C 2020 *Adv. Sci.* **7** 2001823
[11] Huang Z T, Yin C W, Hong Y H, Li H, Hong K B, Kao T S, Shih M H and Lu T C 2021 *Adv. Opt. Mater.* **9** 2100299
[12] Jia X, Wang J, Huang Z, Chu K, Ren K, Sun M, Wang Z, Jin P, Liu K and Qu S 2022 *J. Mater. Chem. C* **10** 680
[13] Jiang D, Li P, Liu B, Huang K, Tao T, Zhi T, Yan Y, Xie Z, Kang J, Zheng Y and Zhang R 2022 *ACS Appl. Nano Mater.* **5** 16971
[14] Vitale F, Repp D, Siefke T, Zeitner U, Peschel U, Pertsch T and Ronning C 2023 *Appl. Phys. Lett.* **122** 101104
[15] Li M, Lu J, Wan P, Jiang M, Mo Y and Pan C 2024 *Adv. Funct. Mater.* **34** 2403840
[16] Chou Y H, Wu Y M, Hong K B, Chou B T, Shih J H, Chung Y C, Chen P Y, Lin T R, Lin C C, Lin S D and Lu T C 2016 *Nano Lett.* **16** 3179
[17] Wang S, Wang X Y, Li B, Chen H Z, Wang Y L, Dai L, Oulton R F and Ma R M 2017 *Nat. Commun.* **8** 1889
[18] Chou Y H, Hong K B, Chung Y C, Chang C T, Chou B T, Lin T R, Arakelian S M, Alodjants A P and Lu T C 2017 *IEEE J. Sel. Top. Quantum Electron.* **23** 1
[19] Lu J, Jiang M, Wei M, Xu C, Wang S, Zhu Z, Qin F, Shi Z and Pan C 2017 *ACS Photonics* **4** 2419
[20] Wang S L, Wang S, Man X K and Ma R M 2020 *Nanophotonics* **9** 3403
[21] Wang R, Xu C X, You D T, Wang X X, Chen J P, Shi Z L, Cui Q N and Qiu T 2021 *Nanoscale* **13** 6780
[22] Chang S W, Lin T R and Chuang S L 2010 *Opt. Express* **18** 15039
[23] Bennett B R, Soref R A and Delalamo J A 1990 *IEEE J. Quantum Electron.* **26** 113